CHEMISTRY OF MATERIALS

pubs.acs.org/cm

Article

Thiol–Yne Crosslinked Nanocomposite Hyaluronic Acid Hydrogels as In Situ-Forming Bone Grafts for the Treatment of Irregular Bone Defects

Alessia Lo Re, Yanmiao Fan, Giovanna Pitarresi, Fabio Salvatore Palumbo, Giuseppina Biscari, Michael Malkoch,* and Calogero Fiorica

Cite This: *Chem. Mater.* 2025, 37, 9440–9450

Read Online

ACCESS | Metrics & More | Article Recommendations | Supporting Information

ABSTRACT: Biopolymer-based nanocomposite injectable hydrogels represent an optimal solution for bone filling and regeneration, providing an effective tool for treating bone fractures or defects, particularly in the maxillofacial and calvarial regions. To overcome the typical limitations of biopolymer-based hydrogels, such as excessive swelling and rapid degradation, this study presents a series of hydrogels synthesized through photoinduced thiol–yne click chemistry between alkyne-functionalized hyaluronic acid (HA) and ethoxylated trimethylolpropane tris(3-mercaptopropionate) (ETTMP). The viscoelastic properties of the gelling solution enable the incorporation of nanohydroxyapatite (nHAp) at concentrations ranging from 10 to 30 wt % relative to the hyaluronan derivative. Gelation occurs within seconds upon blue light irradiation (405 nm) by using a commercial dental lamp. The resulting hydrogels retain approximately 80% of their initial weight after 28 days of incubation in phosphate buffer, while maintaining a stable swelling degree throughout the same period. Following the photoinduced gelation, hydrogels exhibit optimal viscoelastic behavior as well as good adhesiveness to various materials and tissues. Micro-CT analyses confirm that the hydrogels maintain their structural integrity and optimal filling properties over 28 days of incubation in ex vivo bone specimens. Furthermore, cytocompatibility studies conducted on preosteoblastic cells demonstrated 100% cell viability after 48 h of incubation, highlighting the excellent biocompatibility of the developed hydrogels. Preliminary mineralization studies using mesenchymal stem cells and Alizarin Red showed signs, revealing that the presence of hydroxyapatite confers osteogenic properties to the sample

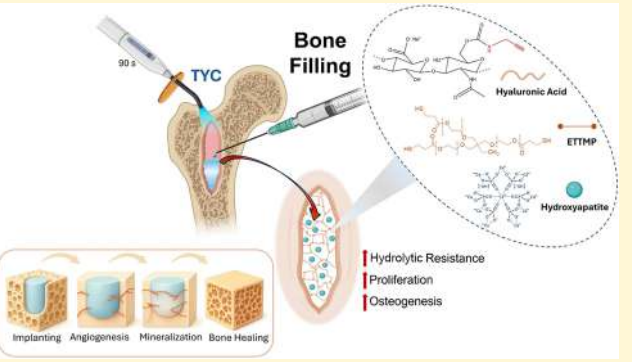

1. INTRODUCTION

Bones provide a vital protective function for the internal organs of the human body, ensuring the maintenance of normal life activities and possessing a natural capacity for regeneration.[1] Critical bone defects caused by trauma, tumors, and frequent pathological conditions such as osteomyelitis,[2] osteoporosis,[3] and osteonecrosis[4] represent a significant challenge in modern clinical practice. To address these issues, research has focused on the development of biocompatible biomaterials, innovative cell therapies, and bioactive molecules to improve bone healing quality, reduce recovery time, and increase surgical success rates. Identifying effective bone regeneration strategies improves patient quality of life and reduces healthcare costs associated with prolonged treatments and complications.[1,5] Bone scaffold materials composed of bioceramics or metals exhibit favorable mechanical properties similar to those of natural bone and have found extensive application in the domain of orthopedic implants. However, these materials currently used in clinics exhibit limited plasticity, difficulty in filling irregular defects, and are therefore unable to fully integrate with bone tissue, resulting in invasive implantation procedures.[6] Bone filling is a procedure used in dentistry and surgery to regenerate or replace missing bone tissue, promoting healing and integration of injected materials into the affected site. This method is used in various diseases or bone defects, such as periodontitis, joint lesions, and calvarial and maxillofacial defects.[1] In the field of bone grafting, a surgical procedure in which bone tissue or a bone substitute is transplanted to stimulate new bone formation in areas of bone loss or defect, bioceramic materials represent a class of synthetic candidates with favorable biocompatibility, osteoconductivity, and high compressive strength. These materials

Received: July 18, 2025
Revised: November 4, 2025
Accepted: November 5, 2025
Published: November 18, 2025

can induce differentiation of bone precursor cells and guide the reconstruction of defective tissues, making them promising candidates for bone repair and tissue regeneration in clinical settings.[7] For instance, nanohydroxyapatite (nHAp) is the most frequently utilized bioactive ceramic material in bone grafting procedures due to its chemical and spatial structure, which is analogous to that of natural bone tissue.[4,8] Tissue engineering represents an alternative and highly effective treatment to overcome various negative postsurgical consequences. Injectable natural biopolymer-based hydrogels that mimic the natural extracellular matrix (ECM) are minimally invasive and can precisely fill complex defects.[4] Among biopolymers used in bone tissue[9] (e.g., gelatin,[10] collagen,[11] sodium alginate,[12,13] and chitosan),[14,15] hyaluronic acid (HA) represents one of the most versatile materials for bone regeneration, providing an extracellular environment for osteogenesis-related cells and initiating multiple cellular signaling pathways in bone regeneration.[6,16,17] HA-based fillers reinforced with nHAp exhibit a mineral composition similar to that of bones and teeth. The combination of HA with nHAp improves filler absorption into the damaged area, helps relieve pain, and reduces rapid HA biodegradation.[18−20]

Recently, Liu et al. developed a nanocomposite hydrogel composed of dopamine-hyaluronic acid, tannic acid, and ZIF-8 particles (dHA/TA/SP) with strong tissue adhesion, antibacterial properties, and enhanced mechanical strength for bone repair. By incorporating simvastatin-loaded ZIF-8 particles coated with hydroxyapatite, the system promotes osteogenesis even if its degradation is relatively fast (around 14 days).[21] While the capacity of the implanted hydrogel to incorporate body fluids can promote tissue regeneration,[6,22,23] excessive swelling can be counterproductive in bone regeneration. Significant swelling at the bone site can hinder optimal interconnection between the implanted material and surrounding tissues, compromising the hydrogel structure and the effectiveness of the regenerative process. To address this, it is essential to design hydrogels with controlled swelling properties, for example, by modifying the cross-linking mechanisms. Hydrogels with high cross-linking density tend to exhibit lower swelling, improving integration with bone tissue and promoting regeneration.[24−26] Additionally, incorporation of inorganic components such as hydroxyapatite can enhance the mechanical properties and reduce swelling, making hydrogels more suitable for bone regeneration applications.[27]

Click chemistry is a rapid and highly selective approach that allows for precise control over bond formation and functionalization. Notably, it operates under mild conditions, without the need for strict temperature or pH control, and avoids the generation of undesired byproducts. Therefore, this approach can be applied under physiological conditions, making it particularly suitable for in situ medical applications.[28,29] Among click-chemistry strategies, thiol−yne chemistry (TYC) is a highly efficient and versatile method that involves UV- or visible-light-induced photopolymerization between thiol and alkyne groups.[30] This approach is known for its exceptional reactivity and ability to generate complex, highly cross-linked networks. The TYC reaction allows creation of homogeneous and well-defined hydrogel networks, often superior to those produced by conventional (meth)-acrylate-based systems, and shows controlled swelling and degradation profiles.[31−33]

Pérez-Madrigal et al. developed a hydrogel for soft tissue regeneration using thiol−yne click chemistry. The system combines sodium alginate with hyaluronic acid (HA) functionalized with thiol groups, cross-linked via a bifunctional linker bearing terminal alkynes. The resulting hydrogel is biocompatible, injectable, and mechanically tunable, making it suitable for soft tissue applications.[34] This study highlights the potential of thiol−yne chemistry in the design of advanced, customizable biomaterials. To date, no HA-based system using this chemistry has been reported for bone tissue engineering, suggesting unexplored opportunities in this field.

In this study, we utilized photoactivated thiol−yne chemistry (TYC) to develop HA-based, covalently cross-linked hydrogel networks loaded with nHAp for potential use as bone fillers in the treatment of irregular bone defects. Alkyne-modified HA was cross-linked with a trifunctional thiol cross-linker using two different molar ratios between thiol groups and the alkyne-functionalized polysaccharide backbone. The presence of varying amounts of nHAp in the precursor gelling solution did not adversely affect the gelation time or hydrogel stability. Incorporation of nHAp, a bioactive ceramic, enhanced the compressive modulus, confirming the positive effect of the doping agent on the physicochemical and mechanical properties of the hydrogels. Ex vivo studies on bone specimens, conducted using a selected sample, demonstrated the feasibility of the proposed injectable bone-filling approach and highlighted the hydrogel's stability upon contact with bone for up to 28 days. In vitro cytocompatibility tests using the murine preosteoblast MC3T3-E1 cell line confirmed the material's safety, while FD-MSC differentiation suggested its potential osteoinductive properties.

2. EXPERIMENTAL SECTION

2.1. Materials. Sodium hyaluronate, concentrated hydrochloric acid (37%), tetrabutylammonium hydroxide (TBA−OH), bis(4-nitrophenyl carbonate) (4-NPBC), propargylamine, sodium chloride (NaCl), anhydrous dimethyl sulfoxide (DMSOa), hydroxyapatite nanopowder (nHAp), Dowex 50WX8 resin, phosphate buffer (Dulbecco's Phosphate-Buffered Saline, DPBS), lithium phenyl-2,4,6-trimethylbenzoylphosphinate (LAP), and deuterium oxide (D_2O) were purchased from Sigma-Aldrich (Italy). Trimethylolpropane tris(3-mercaptopropionate) (TMP-$(SH)_3$/ETTMP) was purchased from Bruno Bock. For the tests of cell viability, Dulbecco's Modified Eagle Medium (DMEM), fetal bovine serum (FBS), and the mixture of antibiotics penicillin/streptomycin were purchased from Euroclone. Low-glucose DMEM was purchased from PAN Biotech. MTS reagent (CellTiter AQueous One Solution Cell Proliferation Assay) was purchased from Promega, Milan, Italy. Acridine Orange (AO), ethidium bromide (EB), Alizarin Red S (ARS) staining kit, dexamethasone, L-ascorbic acid, and β-glycerophosphate were obtained from Merck. Human fetal dermal mesenchymal stromal cells (FD-MSCs) were isolated from fetal dermis in accordance with a protocol approved by ISMETT's Institutional Research Review Board (IRRB) and ethics committee (IRRB/00/15), using a nonenzymatic tissue outgrowth technique, as described by Chinnici et al.[35]

2.2. Synthesis of Hyaluronic Acid−Alkyne Derivative (HY). Low molecular weight hyaluronic acid tetrabutylammonium salt (HA-TBA) was produced as previously reported.[36,37] Briefly, HA was prepared from high molecular weight hyaluronic acid by acidic degradation. The tetrabutylammonium salt of HA (HA-TBA) was produced as previously described to allow its dispersion in organic solvents.[38,39] HY was synthesized by dissolving HA-TBA (1 g) in DMSO at a concentration of 1% w/v and heating the solution to 40 °C.

4-Nitrophenyl carbonate (4-NPBC) was then added to achieve a molar ratio of 0.5 with respect to the repeating units of HA-TBA.

https://doi.org/10.1021/acs.chemmater.5c01899
Chem. Mater. 2025, 37, 9440−9450

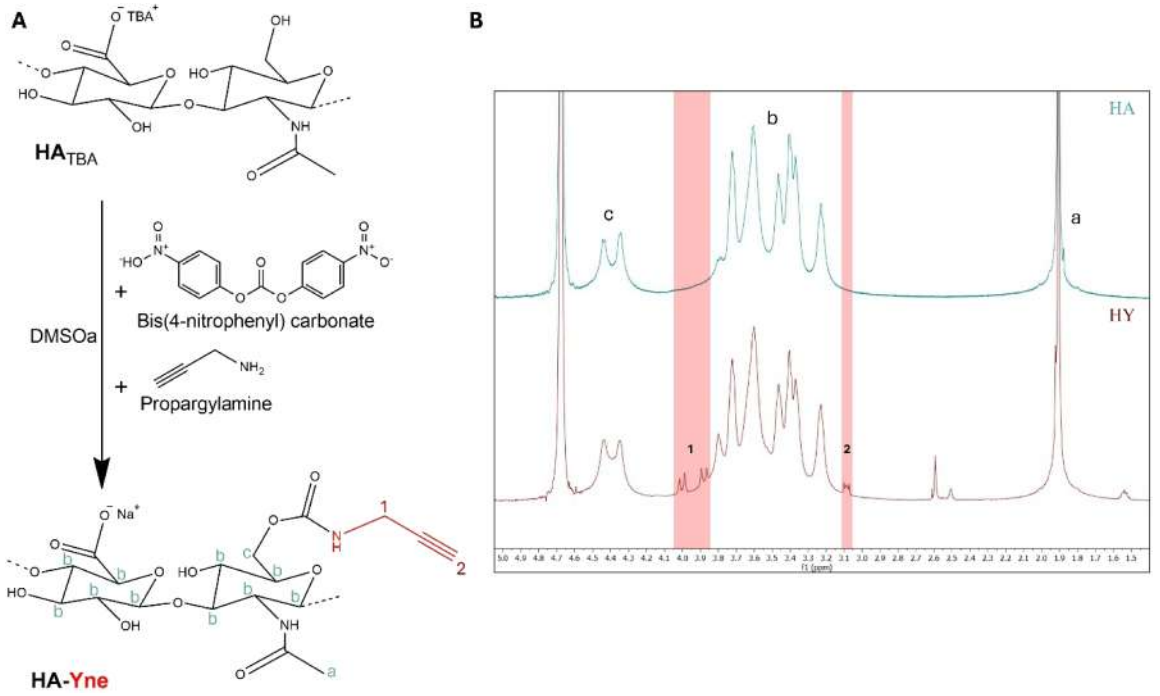

Figure 1. (A) Schematic illustration of HY synthesis. (B) ^{1}H NMR spectra of HA and HY in D_2O.

After 4 h of activation, propargylamine was added at a 5-fold molar excess relative to 4-NPBC, and the reaction was allowed to proceed for 24 h under continuous stirring at 40 °C. The product was purified by dialysis (3.5 kDa cutoff) against 0.5 M NaCl solution for 2 days, followed by dialysis against Milli-Q water for an additional 3 days. The final HY sodium salt was recovered as a white solid by freeze-drying, with a yield of 82% relative to the initial HA-TBA mass.

^{1}H NMR spectroscopy was performed on a 400 MHz Bruker Avance III instrument using deuterated solvents (D_2O). ^{1}H NMR spectra were referenced to the residual solvent peak of D_2O at δ 4.79. The spectra were analyzed with MestreNova. The degree of propargylamine derivatization was calculated as the ratio between the area of the peaks in the range of 4.05−3.85 ppm, attributable to its CH_2 groups (Figure 1B) and the area of the peak at 1.9 ppm, which corresponds to the methyl protons of the *N*-acetyl-D-glucosamine residues.

2.3. HY and ETTMP (YE) and Composite (YE@nHAp) Hydrogel Production. YE hydrogels were synthesized via photo-initiated thiol−yne click chemistry (TYC) between the alkyne groups of HY and the thiol groups of TMP−$(SH)_3$. HY was dissolved in Milli-Q water at room temperature, and TMP−$(SH)_3$ was subsequently added to achieve alkyne-to-thiol molar ratios of 1:2. LAP was introduced as a photoinitiator at a concentration of 0.3% w/v. For all formulations, the final HY concentration was 10% w/v. In the case of the nanocomposite hydrogels, nHAp was incorporated at varying weight ratios relative to HY (10%, 20%, and 30% w/w) and thoroughly mixed using vortexing. Cross-linking was carried out in a cylindrical mold using a portable high-performance LED curing lamp (Bluephase 20i, Ivoclar Vivadent AG, Liechtenstein), emitting dominant wavelengths of 400 and 470 nm with an intensity of 1200 mW/cm^2. The curing process involved three pulses of 30 s each.

Complete TYC cross-linking was verified using the Ellman assay. A DTNB (5,5′-dithiobis(2-nitrobenzoic acid)) solution was prepared in PBS buffer (pH 8) at a concentration of 2 mg/mL and kept in the dark. All freeze-dried hydrogels, HY, and the thiol cross-linker (at different concentrations, 480−7 μg/mL) were placed in PBS buffer (1 mL, pH 8) and gently vortexed.

Then, 200 μL of DTNB solution was added to each sample, gently vortexed, and incubated at room temperature for 15 min in the dark. After this time, the absorbance of the yellow-colored TNB product was measured at 412 nm using an Infinite M200 (Tecan, Switzerland) plate reader. The known thiol concentration standard curve was used to determine the free thiol concentration in the samples, as shown in Table S1.

The morphological characterization of the hydrogels was carried out by scanning electron microscopy (SEM) using a field-emission scanning electron microscope (S-4800, Hitachi, Tokyo, Japan). Cross-sectional freeze-dried samples were coated with platinum using a high-resolution sputter coater (208HR, Cressington, Watford, UK) prior to imaging (Figure 3).

Morphological changes in YE and YE + 30% nHAp hydrogels following enzymatic degradation were also analyzed under the same conditions. The pore size distribution was determined from SEM micrographs using **ImageJ** software (NIH, Bethesda, MD, USA) (Figure S3B).

2.4. Swelling, Hydrolytic, and Enzymatic Degradation. To conduct swelling studies, the freeze-dried hydrogels formed with 50 μL of precursor solution were accurately weighed, immersed in 2 mL of PBS (pH = 7.4, 0.01 M, NaCl 0.154 M), and incubated at 37 °C. At different time points, the swollen hydrogels were weighed, and the swelling ratio percentage (SR%) was calculated according to the following equation:

$$\mathrm{SR}\ (\%) = \frac{W_s - W_d}{W_d} \times 100 \tag{1}$$

where W_s is the weight of the swollen hydrogel and W_d is the starting weight of the freeze-dried hydrogel. Experiments were performed in triplicate.

To determine hydrogels' hydrolytic stability, 50 μL of freeze-dried samples were weighed to determine their initial weight (W_i) and incubated in PBS (2 mL) at 37 °C. At scheduled time points, hydrogel samples were washed twice with Milli-Q water, then freeze-dried, and weighed to determine their final mass (W_f). Experiments were performed in sextuplicate. The degradation rate of the hydrogels at each time point was expressed as the recovered weight percentage (W_r%) calculated using the following equation:

$$W_r\ (\%) = \frac{W_f}{W_i} \times 100 \tag{2}$$

To evaluate the enzymatic stability of the hydrogels, 50 μL of freeze-dried samples were initially weighed to determine their initial

https://doi.org/10.1021/acs.chemmater.5c01899
Chem. Mater. 2025, 37, 9440−9450

mass (W_i) and subsequently incubated in 2 mL of PBS containing hyaluronidase (100 U/mL) at 37 °C. At predetermined time intervals, the samples were collected, thoroughly rinsed five times with Milli-Q water to remove enzyme residues, freeze-dried again, and weighed to determine their final mass (W_f). The degradation of the hydrogels over time was expressed as the percentage of recovered weight (W_r%), calculated according to eq 2. Experiments were performed in triplicate (Figure S3A).

2.5. Rheological Characterization. Rheology measurements were conducted at 25 °C using a Discovery Hybrid Rheometer 2 instrument from TA Instruments. Oscillation amplitude of dispersion, flow sweep, and time sweep measurements were performed on triplicate samples placed on a parallel plate with a 20 mm diameter upper geometry.

Hydrogel frequency sweeps and oscillation amplitude tests were performed on triplicate samples using a parallel plate with an 8 mm diameter crosshatched upper geometry. The LVE (Linear Viscoelastic) region was preliminarily evaluated by amplitude sweep experiments, applying a constant frequency of 0.5 rad/s and an oscillation strain % ranging from 1 to 500%. Furthermore, viscoelastic properties were evaluated by performing a frequency range of 0.1−100 rad/s at a fixed shear strain % within the LVE region (10%) to measure the dynamic storage (G') and loss (G'') moduli.

Photorheology analyses were conducted using the same instrument, equipped with a parallel flat plate geometry with a 20 mm diameter and a UV LED module.

2.6. Compression Testing of Hydrogels. To evaluate the mechanical properties of the YE and composite scaffolds, samples were molded in plastic syringes with an inner diameter of 4.5 mm and a height of 5.5 mm. The compressive strength of the hydrogels was measured by using uniaxial compression tests. The samples were then evaluated using a 4-cell mechanical bioreactor (Bose Biodynamic 3100) at a crosshead speed of 10 mm/min until failure, with a 220 N load cell.

2.7. In Vitro Bone Filling Experiment. The YE + 30% nHAp hydrogel was applied to a surgically induced bone defect in a porcine metacarpal, created with a scalpel under controlled conditions. The hydrogel solution was delivered into the defect using a syringe equipped with a 21G needle and subsequently photo-cross-linked via exposure to high-energy visible (HEV) light for 90 s using a hand-held dental curing lamp.

To further assess the hydrogel's macroscopic stability under conditions simulating the in vivo environment, 300 μL of the YE + 30% formulation was injected into perforated equine bone specimens (cylindrical geometry, 1 cm diameter × 0.5 cm height). Postinjection, the samples were incubated in 6 mL of phosphate-buffered saline (PBS) at 37 °C.

At defined time points, specimens were analyzed via micro-computed tomography (Micro-CT; Skyscan 1272, Bruker) to evaluate the distribution and retention of the hydrogel within the bone matrix.

2.8. Cytocompatibility Studies and Alizarin Red Staining. Cytocompatibility tests were performed by using murine preosteoblasts (MC3T3-E1). Cells were cultured in tissue culture flasks at 37 °C in a humidified atmosphere containing 5% CO_2, using Dulbecco's Modified Eagle Medium (DMEM) supplemented with 10% (v/v) fetal bovine serum (FBS), 4 mM L-glutamine, 100 IU/mL penicillin, and 100 μg/mL streptomycin. After appropriate confluency was reached, the cells were harvested and seeded into 24-well plates at a density of 5×10^5 cells/well in 1 mL of medium and incubated for 24 h.

Subsequently, hydrogel samples (50 μL), previously sterilized under UV light for 30 min, were placed into cell culture inserts and added to each well. After 48 h of coculture, the hydrogels were removed from the wells and cell viability was evaluated by an MTS test following the supplier's instructions. Viability was expressed as a percentage of the control, represented by cells cultured without hydrogels. All experiments were performed in triplicate, and the results are reported as mean ± standard deviation (SD).

The viability was also evaluated through OA/EB staining. In this experiment, fluorescence images were acquired using a Zeiss AxioVert 200 microscope. The AxioVert 200 microscope (Zeiss) was utilized to observe the nuclei of green-stained live cells and red-stained dead cells by employing various fluorescence probes. For the Alizarin red staining experiment, FD-MSCs were seeded at a density of 1×10^4 cells/well (24-well plates) and cocultured with YE or YE + 30% nHAp hydrogel. Hydrogels were sterilized through ultraviolet radiation and incubated with low-glucose growth medium for 24 h to obtain conditioned swollen hydrogels that were incubated with cells in the 24-well plate. After 7 and 28 days, cells were fixed with 4% paraformaldehyde for 15 min at room temperature and incubated with a 0.2% ARS solution (pH = 4.8) for 30 min. Then, the dye was removed, and the cells were washed 5 times with Milli-Q water to remove the excess dye. Lastly, the images were acquired through an optical microscope.

Cells cultured in osteogenic induction medium composed of low-glucose growth medium supplemented with 10% (v/v) fetal bovine serum (FBS), L-glutamine, penicillin, dexamethasone, L-ascorbic acid, and β-glycerophosphate were employed as a positive control.

3. RESULTS AND DISCUSSION

3.1. Synthesis and Characterization of Alkyne−Hyaluronic Acid (HY). Hyaluronic acid derivatives are among the most extensively investigated biomaterials for the development of hydrogels in tissue regeneration, owing to their excellent biocompatibility, tunable physicochemical properties, and capacity to support the repair of various tissues.[40−42] TYC chemistry enables the rapid formation of polymeric networks with high cross-linking density.[30] Compared to other cross-linking methods, the TYC approach enables on-command, chemoselective cross-linking with high monomer conversion, thereby reducing the side reactions commonly encountered in acrylate-based systems.[43] To obtain a hyaluronic acid derivative suitable for cross-linking via TYC, while retaining good water dispersibility and the native polymer's key physicochemical properties, the polysaccharide was functionalized with propargylamine.

The modification was performed using a previously established synthetic strategy based on the selective activation of primary hydroxyl groups in the *N*-acetylglucosamine units with 4-NPBC, followed by nucleophilic substitution with the primary amine.[36,38,41] The resulting alkyne-functionalized HA derivative was designated as HY.

A schematic illustration of the synthesis is presented in Figure 1A. Comparison of the ^{1}H NMR spectra of HY and unmodified HA reveals the appearance of new resonance peaks in the HY spectrum, specifically at 4.05−3.85 ppm (peak 1), corresponding to the methylene protons, and at 3.08 ppm (peak 2) attributable to the alkyne proton of propargylamine.[44,45] These new signals confirm the successful functionalization of hyaluronic acid (Figure 1B). The degree of substitution was determined to be 20 ± 5 mol %.

3.2. Production and Characterization of YE and Composite Hydrogels (YE@nHAp). Four different formulations were prepared using a fixed molar ratio of 1:2 (alkyne:thiol) by dissolving HY and TMP−$(SH)_3$ in deionized water in the presence of LAP and varying amounts of nHAp. The nHAp unloaded hydrogel without nHAp was named YE, while nanocomposite samples (YE@nHAp) were labeled as YE + 10%, YE + 20%, and YE + 30% based on the w/w percentage of nHAp loaded compared to HY.

The TYC cross-linking mechanism can proceed spontaneously under physiological conditions through a radical-mediated two-step addition. Initially, thiyl radicals (RS•) are generated and add to the alkyne triple bond, forming a vinyl

https://doi.org/10.1021/acs.chemmater.5c01899
Chem. Mater. 2025, 37, 9440−9450

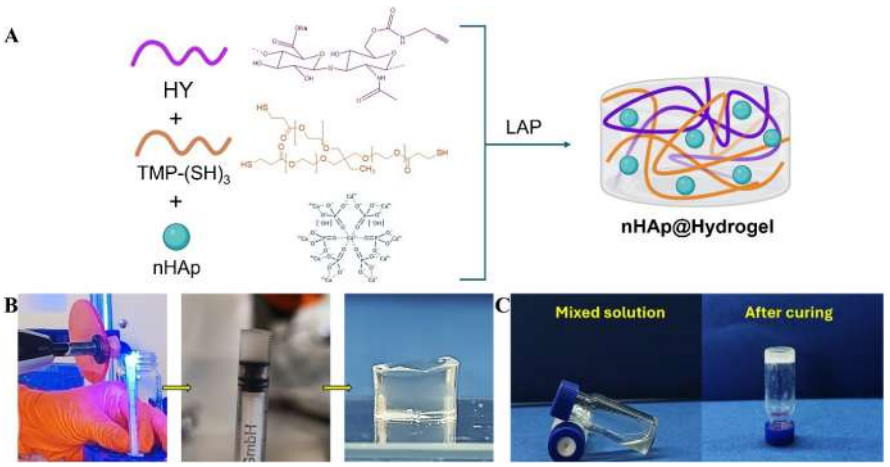

Figure 2. Preparation of HY hydrogels based on photoinduced thiol−yne click chemistry (TYC): (A) A schematic illustration of hydrogel production. (B) Representative pictures of photoinduced gelation with a dental lamp and the obtained hydrogels. (C) Tube inversion after HEV cross-linking.

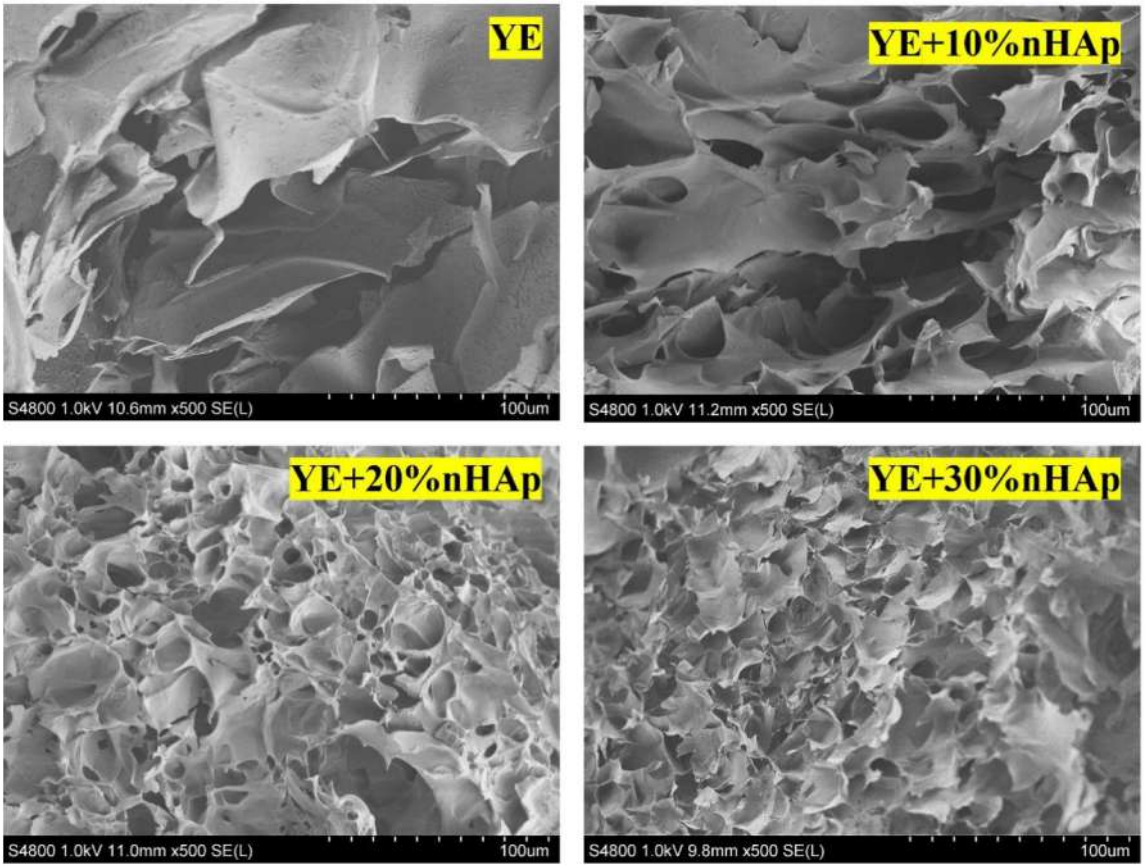

Figure 3. SEM images of freeze-dried YE hydrogels with different nHAp content.

sulfide intermediate. Subsequently, a second thiol adds to this intermediate via radical attack, completing the cross-linking process.[46−48] In line with this, our gel-forming solutions, when left at room temperature under ambient light, underwent spontaneous gelation over time, leading to the formation of soft, loosely structured hydrogels, as confirmed by the vial inversion test (Figure S1).

However, when the same precursor solutions were exposed to 405 nm light in the presence of LAP, rapid and complete gelation occurred within a few seconds, resulting in free-standing, compact, and easily handled hydrogels (Figure 2B−C). This behavior is attributed to the photocatalyzed TYC reaction, which proceeds through a radical-mediated mechanism, maximizing the efficacy of the reaction. This pathway, which requires an alkyne-to-thiol ratio of 1:2, results in the formation of compact polymeric networks with enhanced macroscopic integrity through the complete utilization of all thiol groups present in the mixture.

The ability to control the timing and structure of hydrogel formation is particularly advantageous for bone tissue

https://doi.org/10.1021/acs.chemmater.5c01899
Chem. Mater. 2025, 37, 9440−9450

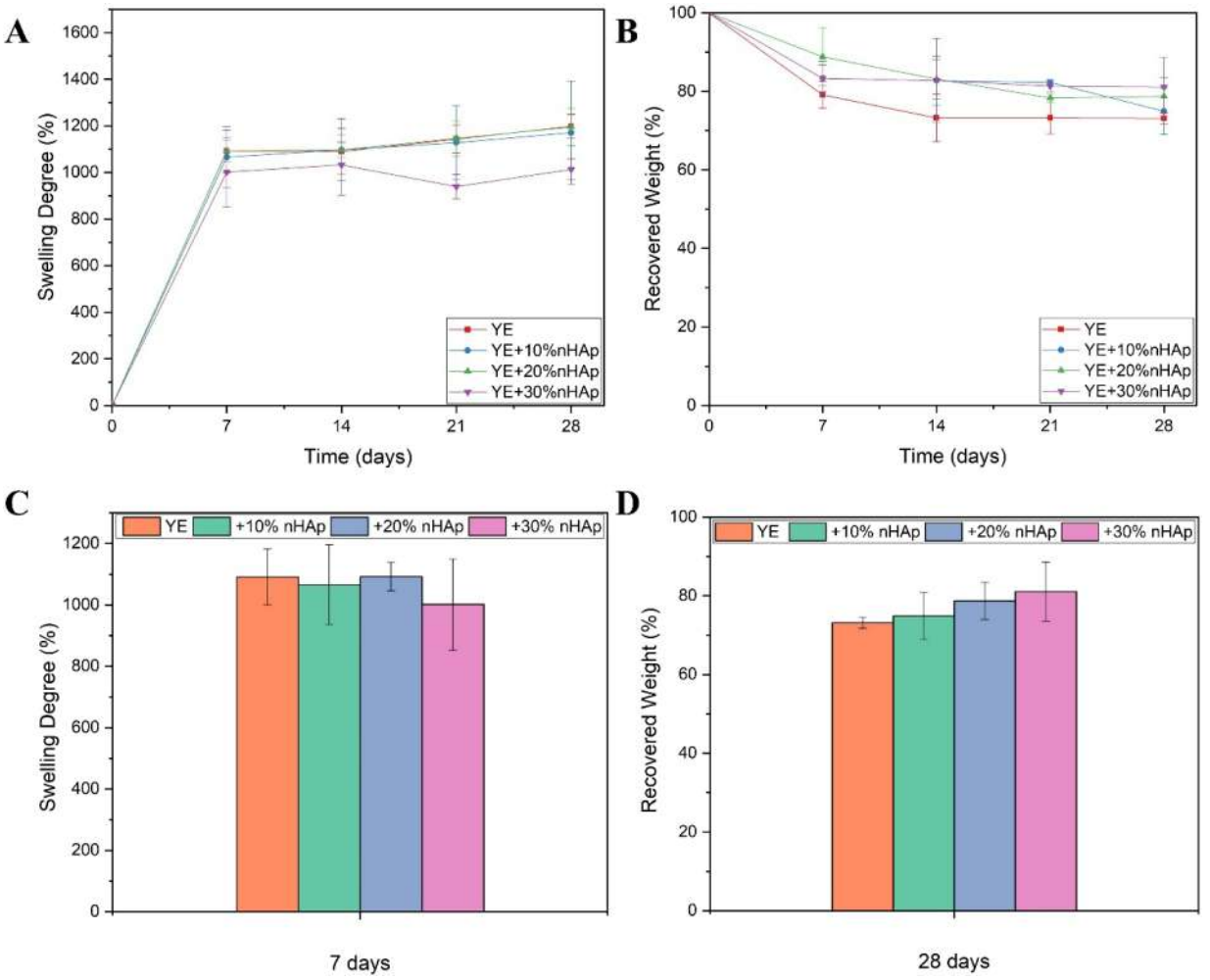

Figure 4. (A) Swelling degree and (B) recovered weight of YE hydrogels with different nHAp contents. (C) Swelling degree of samples compared after 7 days of incubation. (D) Recovered weight (%) of samples compared at 28 days.

engineering applications. An ideal injectable bone filler should conform to the defect sites, fill the void homogeneously, and undergo rapid in situ cross-linking in response to a controllable, externally applied stimulus. Moreover, temporal control over the gelation process is critical to ensuring precise positioning and stabilization of the material.

The formulation strategy meets these criteria by providing a stable, injectable precursor solution with a defined working time (~15 min under ambient conditions), followed by fast and controlled cross-linking upon HEV or UV exposure (90 s). The transition from spontaneous to photoinduced TYC not only accelerates gelation but also enhances the structural and mechanical properties of the resulting hydrogels, making this approach particularly suitable for precise and reliable in situ applications in bone defect repair. Interestingly, the resulting hydrogels exhibited a certain degree of adhesiveness on both biological (pig bones and skin) and nonbiological substrates, such as paper, metal, glass, and plastic, a property particularly noteworthy for a wide range of biomedical applications (Figure S2).

SEM images revealed that all hydrogels exhibited a porous morphology after freeze-drying. Interestingly, the incorporation of nHAp resulted in a more regular and uniform pore distribution (Figure 3). No hydroxyapatite aggregates were detected, confirming the effective dispersion of the bioceramic phase within the gel-forming solution. Furthermore, the denser and more interconnected porous network observed in the composites is expected to contribute to enhanced mechanical stability, a key requirement for bone tissue engineering applications.[14,49]

3.3. Swelling Degree and Hydrolytic Degradation. A key observation from the swelling studies is that all investigated samples absorb a substantial amount of water upon transitioning from the freeze-dried state and exhibit long-term stability in the wet state. More specifically, the equilibrium swelling, achieved in the early stages of incubation, ranged from 900% to 1200% and remained consistent throughout the entire 28-day experimental period. These findings align with previous reports and confirm that the applied cross-linking method yields highly stable hydrogel networks.[50] Such stability is particularly advantageous in bone tissue engineering, where preserving the structural integrity of the implanted material during the healing phase is of critical importance.[3,5,6]

Interestingly, a slight decrease in swelling was observed only in the sample with the highest nHAp content (Figure 4A–C). This comparable behavior suggests that the intrinsic compactness of the polymer network is the primary determinant of water uptake capacity, potentially overshadowing any effects related to the incorporation of nHAp.

https://doi.org/10.1021/acs.chemmater.5c01899
Chem. Mater. 2025, 37, 9440–9450

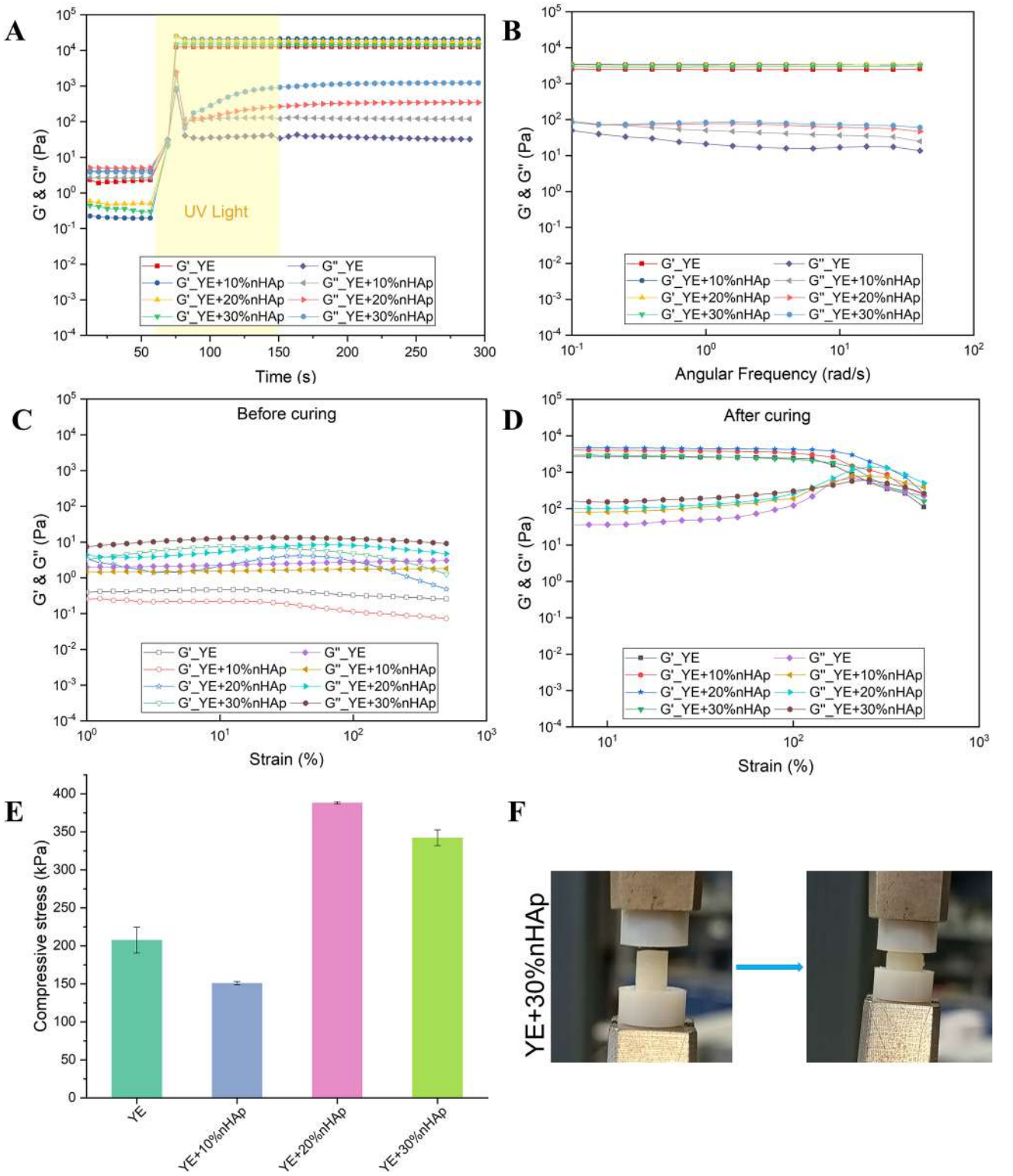

Figure 5. Rheological and mechanical analysis of YE hydrogels with different nHAp weight ratios: (A) photorheology, (B) frequency sweep, (C) amplitude sweep before curing, (D) amplitude sweep after curing, (E) compression moduli from mechanical compression tests, and (F) fatigue resistance of YE + 30% nHAp. Results are presented as mean ± SD from experiments performed in triplicate.

Similarly, hydrolytic degradation studies revealed no statistically significant differences in the recovered weight percentages among the different formulations (Figure 4B). After 28 days of incubation, all hydrogels retained approximately 80% of their initial weight, further supporting their hydrolytic stability and degradation profile, both of which are aligned with the requirements for bone tissue regeneration (Figure 4D). It is worth noting that the reparative phase of bone healing typically occurs within one to 3 weeks in individuals without additional complications or comorbidities.[51,52] Therefore, the observed resistance to hydrolysis exhibited by these hydrogels may be well-aligned with the physiological timeline for bone

https://doi.org/10.1021/acs.chemmater.5c01899
Chem. Mater. 2025, 37, 9440−9450

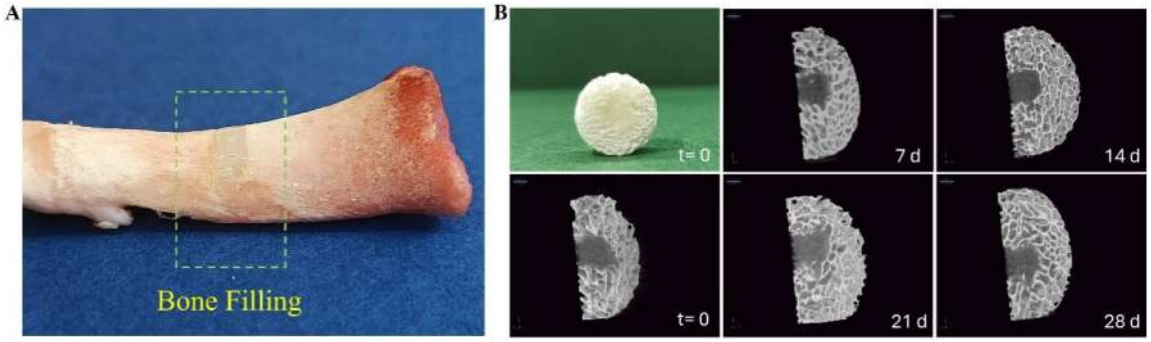

Figure 6. (A) Cured YE + 30% hydrogel within the bone void. (B) Micro-CT cross-section images of equine bone specimens filled with YE + 30% nHAp after 0, 7, 14, 21, and 28 days of incubation in PBS pH 7.4 at 37 °C.

regeneration, corroborating their potential applicability in clinical scenarios.

In vivo, damaged tissues undergoing regeneration are characterized by complex and dynamic conditions (e.g., pH fluctuations, the presence of specific enzymes, and immune cell activity) that are difficult to reproduce in vitro. Such factors can markedly influence the degradation kinetics of the implanted material. To evaluate the sensitivity of the hydrogels to enzymatic degradation, YE and YE + 30% nHAp samples were incubated with hyaluronidase (100 U/mL). The results (Figure S3A) demonstrated that, although the material retained substantial resistance to enzymatic degradation, the residual weight was lower than that observed under purely hydrolytic conditions.

After 7 days of enzymatic exposure, SEM analysis of the scaffold cross-sections revealed a noticeable increase in pore size within both formulations (Figure S3B). Specifically, the average pore size of the YE + 30% nHAp hydrogels increased from 25.37 to 122.27 μm, falling within the 100−300 μm range reported to be optimal for cell infiltration.[14,49,53,54]

3.4. Rheological and Mechanical Properties of Composite Hydrogels. The gelation kinetics of the systems were investigated using photorheology through a time sweep analysis. As shown in Figure 5A, solutions were exposed to irradiation, and both the storage modulus (G') and loss modulus (G'') were monitored to assess the cross-linking process of the hydrogels. The results indicated that cross-linking for the YE and all the nanocomposite hydrogels was initiated upon UV exposure, with the storage modulus reaching a plateau ($\geq 10^4$ Pa) within a few seconds after the irradiation began. The storage modulus of the nanocomposite hydrogels was not significantly different from that of the YE hydrogel, suggesting that the incorporation of nHAp did not alter the gelation kinetics of the system or the viscoelastic properties. The frequency sweep analysis of all the hydrogels, shown in Figure 5B, revealed elastic behavior, and the hydrogels showed the $G' > G''$ across the entire frequency range investigated. Notably, G' remained largely frequency-independent and was more than 1 order of magnitude higher than G''. These results corroborate previous findings, indicating that all hydrogels can be classified as stable and resistant hydrogels.[55]

Oscillation amplitude analysis clearly highlights the effect of cross-linking on the viscoelastic properties of all hydrogels (both with and without nHAp). The solution prior to cross-linking (Figure 5C) shows low values of both G' and G'' (less than 10^1 Pa) over the entire strain range investigated, although G' exceeds G'', indicating the formation of a weakly structured viscoelastic network. However, upon irradiation (Figure 5D), a marked increase of both moduli, of more than 2 orders of magnitude ($G' \geq 10^3$ and $G'' \geq 10^2$), is observed, confirming the formation of a robust cross-linked network. The dominant elastic behavior ($G' > G''$) is preserved, but the significantly higher modulus reflects an increased network stiffness induced by photo-cross-linking. This transition highlights the effectiveness of the photoinduced TYC process in structuring the hydrogels and in transitioning the materials from a soft pregel state to elastic, stable hydrogels.

Compression assessment revealed a significant difference in the mechanical response of the hydrogels under load, despite all samples exhibiting comparable viscoelastic behavior, as indicated by similar G' values in the rheology analyses. The compressive strength of the hydrogels varied with nHAp content: formulations with 10, 20, and 30% w/w nHAp (relative to HY content) yielded values of 151 ± 2.13, 388 ± 1.57, and 342 ± 10.3 kPa, respectively, compared to 208 ± 16.97 kPa for the undoped YE hydrogel (Figure 5E). The sample with the lowest nanoparticle content (10%) demonstrated slightly lower mechanical properties than the undoped hydrogel, likely due to the nanoparticles perturbing the hydrogel entanglement without establishing stabilizing interactions with the polymer chains. In contrast, higher nanoparticle concentrations (20% and 30%) led to a pronounced enhancement of compressive strength, with only a slight variation between them. This mechanical robustness, combined with consistent viscoelastic behavior, represents a significant advantage for bone tissue engineering, where materials must withstand compressive stresses while preserving functional integrity at the defect site. The results obtained are consistent with those reported in similar studies in the literature, confirming the suitability of the material for bone tissue engineering applications.[10,14,53,54] Given that the rheological and mechanical properties of the hydrogels containing 20% and 30% nHAp did not exhibit significant differences, the composite hydrogel with the higher content of osteoinductive agent was selected for further characterization.

The filling of bone defects using a damp porcine bone model was conducted as a proof-of-concept to evaluate the injectability of the hydrogel and its capacity to conformally fill osseous voids. The application of the YE + 30% nHAp hydrogel was conducted on a cavity (10 × 5 × 2 mm) created in a porcine metacarpal bone (Figure 6A). The hydrogel precursor solution was applied to the void via a syringe (21 gauge) and cured with 90 s exposures to high-energy visible light (HEV) from a hand-held dental curing light. The manageable viscosity of the solution enabled effective filling of the bone defect without leakage. Following cross-linking, the

https://doi.org/10.1021/acs.chemmater.5c01899
Chem. Mater. 2025, 37, 9440−9450

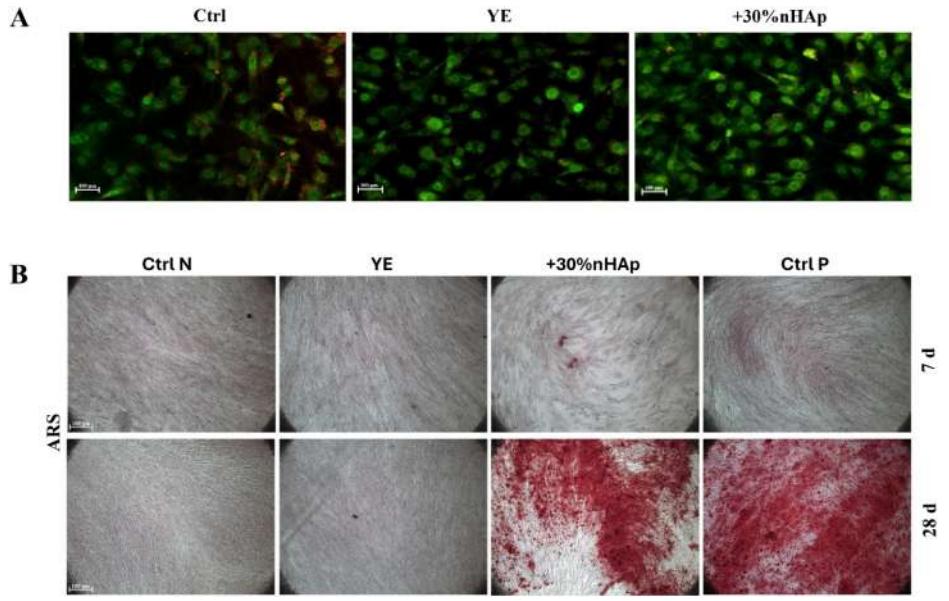

Figure 7. (A) OA/EB staining of MC3T3-E1 after 48 h of culture. (B) Representative optical images of ARS stained after 7 and 28 days for FD-MSCs cultured with YE, YE + 30% nHAp hydrogels, and osteogenic induction medium (Ctrl P).

hydrogel adhered firmly to the cavity in the metacarpal bone, ensuring stable placement and preventing detachment.

In addition, five punched equine bone samples were filled with the nanocomposite hydrogel and incubated under physiological conditions (PBS, 37 °C) to assess whether the material could remain stably retained within the defect site over time (Figure 6B). After 28 days of incubation, Micro-CT cross-sectional images showed that the hydrogel remained within the created cavities, confirming its ability to adhere and persist in the defect area. These results highlight the practical applicability of the system, demonstrating that it can be easily introduced into a bone defect without requiring complex procedures. Moreover, its capacity to remain stable in situ suggests that it can persist at the implantation site for a period potentially sufficient to support and sustain the natural processes of tissue regeneration. This combination of ease of application and functional residence time reinforces its suitability for use in bone repair strategies.

3.5. Cytocompatibility Studies and Alizarin Red Staining. The safety of biomaterials is a pivotal requirement for clinical applications. Using the MTS assay, the hydrogels' impact on MC3T3-E1 cell proliferation was assessed. After 48 h of culture in the presence of the hydrogels, cell viability was assessed using the MTS assay (Figure S4). Cells treated with the samples, both with and without nHAp, showed cell viability levels comparable to those of the control group, confirming the good cytocompatibility of all YE-based hydrogels. To further support these results, AO/EB Live/Dead staining was performed, revealing that the majority of MC3T3-E1 cells appeared to be green, indicating they were alive. The morphology of hydrogel-treated cells was similar to that of the control, as observed under fluorescence microscopy (Figure 7A). As a proof of concept, a preliminary investigation into the potential osteoinductive properties of the nanocomposite hydrogels was conducted using Alizarin Red S staining on FD-MSCs after 7 and 28 days of culture. As shown in Figure 7B, after 28 days, cells cultured in the presence of the nanocomposite hydrogel exhibited calcium deposition comparable to that observed in cells maintained in osteogenic medium. As expected, no mineralization was detected in either the YE hydrogel without nHAp or the negative control group (cells cultured in low-glucose medium). These preliminary results support the hypothesis that the nanocomposite hydrogel may effectively promote bone regeneration in vivo.

4. CONCLUSION

The implementation of thiol−yne cross-linking, achieved through a hyaluronic acid derivative functionalized with alkyne groups, enabled the in situ formation of mechanically robust hydrogels via HEV-curing in only 90 s. This remarkably fast process yielded hydrogels with enhanced resistance to hydrolytic degradation and minimal swelling over the evaluated time frame, which is consistent with the typical duration required for bone regeneration. The mechanical and viscoelastic characteristics of the resulting hydrogels were found to be well-suited for bone void filling applications.

These outcomes are particularly significant, considering the commonly reported limitations associated with hyaluronic acid−based hydrogels, particularly their low mechanical strength and rapid degradation. In vitro biological assays confirmed the excellent cytocompatibility of the system, as well as its capacity to promote mineralization in fetal dermal mesenchymal stem cells (FD-MSCs). Collectively, these findings suggest that the developed hydrogel platform holds considerable promise for further investigation as a bone filler for critical-size bone defect repair.

■ ASSOCIATED CONTENT

Data Availability Statement

Data will be made available upon request.

Supporting Information

The Supporting Information is available free of charge at https://pubs.acs.org/doi/10.1021/acs.chemmater.5c01899.

Additional experimental tables and figures, including Ellman assay, gelation under ambient conditions, additional SEM images, adhesive properties, and cytocompatibility (PDF)

https://doi.org/10.1021/acs.chemmater.5c01899
Chem. Mater. 2025, 37, 9440−9450

AUTHOR INFORMATION

Corresponding Author

Michael Malkoch − *School of Engineering Sciences in Chemistry, Biotechnology and Health (CBH), Department of Fibre and Polymer Technology, Division of Coating Technology, KTH Royal Institute of Technology, Stockholm SE-100 44, Sweden;* orcid.org/0000-0002-9200-8004; Email: malkoch@kth.se

Authors

Alessia Lo Re − *Department of Biological Chemical and Pharmaceutical Science and Technology (STEBICEF), University of Palermo, Palermo 90123, Italy*

Yanmiao Fan − *School of Engineering Sciences in Chemistry, Biotechnology and Health (CBH), Department of Fibre and Polymer Technology, Division of Coating Technology, KTH Royal Institute of Technology, Stockholm SE-100 44, Sweden*

Giovanna Pitarresi − *Department of Biological Chemical and Pharmaceutical Science and Technology (STEBICEF), University of Palermo, Palermo 90123, Italy;* orcid.org/0000-0002-0815-9142

Fabio Salvatore Palumbo − *Department of Biological Chemical and Pharmaceutical Science and Technology (STEBICEF), University of Palermo, Palermo 90123, Italy;* orcid.org/0000-0001-6196-7782

Giuseppina Biscari − *Department of Biological Chemical and Pharmaceutical Science and Technology (STEBICEF), University of Palermo, Palermo 90123, Italy*

Calogero Fiorica − *Department of Biological Chemical and Pharmaceutical Science and Technology (STEBICEF), University of Palermo, Palermo 90123, Italy;* orcid.org/0000-0002-5169-4036

Complete contact information is available at: https://pubs.acs.org/10.1021/acs.chemmater.5c01899

Author Contributions

A.L.R. performed most of the experimental part; A.L.R. and G.B. conducted rheological studies; Y.F. acquired SEM images; M.M. and C.F. analyzed the data and supervised the work. All authors have read and approved the manuscript.

Notes

The authors declare no competing financial interest.

ACKNOWLEDGMENTS

The authors would like to thank Dr. Paolo Bonomo and Dr. Elisabetta Morici of the Advanced Technologies Network Center (ATeN Center) of the University of Palermo for their kind technical support in the acquisition of SEM and Micro-CT images and in the mechanical compression tests on the hydrogels, respectively.

REFERENCES

(1) Zhang, S.; Li, X.; Li, C.; Cong, H.; Yu, B. Research progress of injectable hydrogels in the treatment of bone tissue diseases. *Chem. Eng. J.* **2024**, *498*, 155139.

(2) Zhong, C.; Wu, Y.; Lin, H.; Liu, R. Advances in the antimicrobial treatment of osteomyelitis. *Composites, Part B* **2023**, *249*, 110428.

(3) Ma, Y.; et al. The hyaluronic acid-gelatin hierarchical hydrogel for osteoporotic bone defect repairment. *Int. J. Biol. Macromol.* **2024**, *276*, 133821.

(4) Luo, Y.; et al. Immune regulation enhances osteogenesis and angiogenesis using an injectable thiolated hyaluronic acid hydrogel with lithium-doped nano-hydroxyapatite (Li-nHA) delivery for osteonecrosis. *Mater. Today Bio.* **2024**, *25*, 100976.

(5) Li, M.; Wu, H.; Gao, K.; Wang, Y.; Hu, J.; Guo, Z.; Hu, R.; Zhang, M.; Pang, X.; Guo, M.; et al. Smart Implantable Hydrogel for Large Segmental Bone Regeneration. *Adv. Healthcare Mater.* **2024**, *13* (32), 2402916.

(6) Rubina, A.; et al. Injectable mineralized Sr-hydroxyapatite nanoparticles-loaded ε-polylysine-hyaluronic acid composite hydrogels for bone regeneration. *Int. J. Biol. Macromol.* **2024**, *280*, 135703.

(7) Jiang, S.; Wang, M.; He, J. A review of biomimetic scaffolds for bone regeneration: Toward a cell-free strategy. *Bioeng. Transl. Med.* **2021**, *6* (2), No. e10206.

(8) Zhang, Q.; Ma, L.; Ji, X.; He, Y.; Cui, Y.; Liu, X.; Xuan, C.; Wang, Z.; Yang, W.; Chai, M.; et al. High-Strength Hydroxyapatite Scaffolds with Minimal Surface Macrostructures for Load-Bearing Bone Regeneration. *Adv. Funct. Mater.* **2022**, *32* (33), 2204182.

(9) Zheng, Y.; Ke, Z.; Hu, G.; Tong, S. Hydrogel promotes bone regeneration through various mechanisms: A Review. *Biomed. Eng./Biomed. Tech.* **2025**, *70*, 103−114.

(10) Hou, X.; et al. The hydroxyapatite microtubes enhanced GelMA hydrogel scaffold with inner "pipeline framework" structure for bone tissue regeneration. *Composites, Part B* **2022**, *228*, 109396.

(11) Jiang, Q.; et al. Injectable NGF-loaded double crosslinked collagen/hyaluronic acid hydrogels for irregular bone defect repair via neuro-guided osteogenic process. *Chem. Eng. J.* **2024**, *497*, 154627.

(12) Huang, S.; Wang, Z.; Sun, X.; Li, K. Bone Morphogenetic Protein 7-Loaded Gelatin Methacrylate/Oxidized Sodium Alginate/Nano-Hydroxyapatite Composite Hydrogel for Bone Tissue Engineering. *Int. J. Nanomed.* **2024**, *19*, 6359−6376.

(13) Angili, S. N.; et al. Fabrication and finite element simulation of antibacterial 3D printed Poly L-lactic acid scaffolds coated with alginate/magnesium oxide for bone tissue regeneration. *Int. J. Biol. Macromol.* **2023**, *224*, 1152−1165.

(14) Jiang, Z.; et al. Investigating the anti-inflammatory and bone repair-promoting effects of an injectable porous hydrogel containing magnesium ions in a rat periodontitis mode. *Smart Mater. Med.* **2024**, *5*, 207−220.

(15) Zhou, T.; et al. An injectable carboxymethyl chitosan hydrogel scaffold formed via coordination bond for antibacterial and osteogenesis in osteomyelitis. *Carbohydr. Polym.* **2024**, *324*, 121466.

(16) Kogan, G.; Šoltés, L.; Stern, R.; Gemeiner, P. Hyaluronic acid: A natural biopolymer with a broad range of biomedical and industrial applications. *Biotechnol. Lett.* **2006**, *29*, 17−25.

(17) Zhang, H.; et al. Bone/cartilage targeted hydrogel: Strategies and applications. *Bioact. Mater.* **2023**, *23*, 156−169.

(18) Maji, S.; Agarwal, T.; Das, J.; Maiti, T. K. Development of gelatin/carboxymethyl chitosan/nano-hydroxyapatite composite 3D macroporous scaffold for bone tissue engineering applications. *Carbohydr. Polym.* **2018**, *189*, 115−125.

(19) Dennis, S. C.; Whitlow, J.; Detamore, M. S.; Kieweg, S. L.; Berkland, C. J. Hyaluronic-Acid−Hydroxyapatite Colloidal Gels Combined with Micronized Native ECM as Potential Bone Defect Fillers. *Langmuir* **2017**, *33*, 206−218.

(20) Subramaniam, S.; Fang, Y.-H.; Sivasubramanian, S.; Lin, F.-H.; Lin, C. Hydroxyapatite-calcium sulfate-hyaluronic acid composite encapsulated with collagenase as bone substitute for alveolar bone regeneration. *Biomaterials* **2016**, *74*, 99−108.

(21) Liu, J.; et al. Nanocomposite hyaluronic acid adhesive hydrogel with controllable drug release for bone regeneration. *Int. J. Biol. Macromol.* **2024**, *274*, 133362.

(22) Faruq, O.; Kim, B.; Padalhin, A.R.; Lee, G.H.; Lee, B.T. A hybrid composite system of biphasic calcium phosphate granules loaded with hyaluronic acid−gelatin hydrogel for bone regeneration. *J. Biomater Appl.* **2017**, *32* (4), 433−445.

(23) Burdick, J. A.; Anseth, K. S. Photoencapsulation of osteoblasts in injectable RGD-modified PEG hydrogels for bone tissue engineering. *Biomaterials* **2002**, *23*, 4315−4323.

(24) Miao, Y.; Liu, X.; Luo, J.; Yang, Q.; Chen, Y.; Wang, Y.; et al. Double-Network DNA Macroporous Hydrogel Enables Aptamer-

Directed Cell Recruitment to Accelerate Bone Healing. *Adv. Sci.* **2024**, *11* (1), 2303637.
(25) Zhao, D.; et al. Degradation-Kinetics-Controllable and Tissue-Regeneration-Matchable Photocross-linked Alginate Hydrogels for Bone Repair. *ACS Appl. Mater. Interfaces* **2022**, *14*, 21886−21905.
(26) Feng, W.; Wang, Z. Tailoring the Swelling-Shrinkable Behavior of Hydrogels for Biomedical Applications. *Adv. Sci.* **2023**, *10* (28), 2303326.
(27) Dhivya, S.; Saravanan, S.; Sastry, T. P.; Selvamurugan, N. Nanohydroxyapatite-reinforced chitosan composite hydrogel for bone tissue repair in vitro and in vivo. *J. Nanobiotechnol.* **2015**, *13* (1), 40.
(28) Lin, J.; Fan, Y.; Hutchinson, D. J.; Malkoch, M. Soft Hydroxyapatite Composites Based on Triazine−Trione Systems as Potential Biomedical Engineering Frameworks. *ACS Appl. Mater. Interfaces* **2023**, *15*, 7329−7339.
(29) Sanz Del Olmo, N.; et al. Antibacterial Hydrogel Adhesives Based on Bifunctional Telechelic Dendritic-Linear−Dendritic Block Copolymers. *J. Am. Chem. Soc.* **2024**, *146*, 17240−17249.
(30) Arseneault, M.; Granskog, V.; Khosravi, S.; Heckler, I. M.; Mesa-Antunez, P.; Hult, D.; Zhang, Y.; Malkoch, M. The Dawn of Thiol-Yne Triazine Triones Thermosets as a New Material Platform Suited for Hard Tissue Repair. *Adv. Mater.* **2018**, *30* (52), 1804966.
(31) Ligon, S. C.; Liska, R.; Stampfl, J.; Gurr, M.; Mülhaupt, R. Polymers for 3D Printing and Customized Additive Manufacturing. *Chem. Rev.* **2017**, *117*, 10212−10290.
(32) Bagheri, A.; Jin, J. Photopolymerization in 3D Printing. *ACS Appl. Polym. Mater.* **2019**, *1*, 593−611.
(33) Zanon, M.; et al. Photocurable Thiol−yne Alginate Hydrogels for Regenerative Medicine Purposes. *Polymers* **2022**, *14*, 4709.
(34) Pérez-Madrigal, M. M.; et al. Robust alginate/hyaluronic acid thiol−yne click-hydrogel scaffolds with superior mechanical performance and stability for load-bearing soft tissue engineering. *Biomater. Sci.* **2020**, *8*, 405−412.
(35) Chinnici, C. M.; et al. Isolation and Characterization of Multipotent Cells from Human Fetal Dermis. *Cell Transplant.* **2014**, *23*, 1169−1185.
(36) Fiorica, C.; et al. A new hyaluronic acid pH sensitive derivative obtained by ATRP for potential oral administration of proteins. *Int. J. Pharm.* **2013**, *457*, 150−157.
(37) Shu, X. Z.; Liu, Y.; Luo, Y.; Roberts, M. C.; Prestwich, G. D. Disulfide Cross-Linked Hyaluronan Hydrogels. *Biomacromolecules* **2002**, *3*, 1304−1311.
(38) Palumbo, F. S.; et al. Chemical hydrogels based on a hyaluronic acid-graft-α-elastin derivative as potential scaffolds for tissue engineering. *Mater. Sci. Eng.* **2013**, *33*, 2541−2549.
(39) Palumbo, F. S.; Pitarresi, G.; Mandracchia, D.; Tripodo, G.; Giammona, G. New graft copolymers of hyaluronic acid and polylactic acid: Synthesis and characterization. *Carbohydr. Polym.* **2006**, *66*, 379−385.
(40) Martorana, A.; et al. Fabrication of silver nanoparticles by a diethylene triamine-hyaluronic acid derivative and use as antibacterial coating. *Carbohydr. Polym.* **2022**, *295*, 119861.
(41) Palumbo, F. S.; et al. In situ forming hydrogels of new amino hyaluronic acid/benzoyl-cysteine derivatives as potential scaffolds for cartilage regeneration. *Soft Matter* **2012**, *8*, 4918−4927.
(42) Palumbo, F. S.; et al. Construction and evaluation of sponge scaffolds from hyaluronic acid derivatives for potential cartilage regeneration. *J. Mater. Chem. B* **2014**, *2*, 3243−3253.
(43) Steudter, T.; Lam, T.; Pirmahboub, H.; Stoppel, C.; Kloke, L.; Pearson, S.; Del Campo, A.; et al. A Comparative Study between Thiol-Ene and Acrylate Photocrosslinkable Hyaluronic Acid Hydrogel Inks for Digital Light Processing. *Macromol. Biosci.* **2025**, *25* (3), 2400535.
(44) Yang, H.; et al. Theranostic nanoparticles with aggregation-induced emission and mri contrast enhancement characteristics as a dual-modal imaging platform for image-guided tumor photodynamic therapy. *Int. J. Nanomed.* **2020**, *15*, 3023−3038.
(45) Huerta-Angeles, G.; et al. Synthesis of highly substituted amide hyaluronan derivatives with tailored degree of substitution and their crosslinking via click chemistry. *Carbohydr. Polym.* **2011**, *84*, 1293−1300.
(46) Fairbanks, B. D.; Scott, T. F.; Kloxin, C. J.; Anseth, K. S.; Bowman, C. N. Thiol−Yne Photopolymerizations: Novel Mechanism, Kinetics, and Step-Growth Formation of Highly Cross-Linked Networks. *Macromolecules* **2009**, *42*, 211−217.
(47) Roppolo, I.; et al. Thiol−yne chemistry for 3D printing: Exploiting an off-stoichiometric route for selective functionalization of 3D objects. *Polym. Chem.* **2019**, *10*, 5950−5958.
(48) Sradha, A.; Sariga, S.; George, L.; Varghese, A. Advancements in thiol-yne click chemistry: Recent trends and applications in polymer synthesis and functionalization. *Mater. Today Chem.* **2024**, *38*, 102112.
(49) Xu, Y.; et al. Stratified-structural hydrogel incorporated with magnesium-ion-modified black phosphorus nanosheets for promoting neuro-vascularized bone regeneration. *Bioact. Mater.* **2022**, *16*, 271−284.
(50) Macdougall, L. J.; Pérez-Madrigal, M. M.; Arno, M. C.; Dove, A. P. Nonswelling Thiol−Yne Cross-Linked Hydrogel Materials as Cytocompatible Soft Tissue Scaffolds. *Biomacromolecules* **2018**, *19*, 1378−1388.
(51) Islam, O.; et al. Development and Duration of Radiographic Signs of Bone Healing in Children. *Am. J. Roentgenol.* **2000**, *175*, 75−78.
(52) Kalfas, I. H. Principles of bone healing. *Neurosurg. Focus FOC* **2001**, *10*, 1−4.
(53) Chatterjee, K.; et al. The effect of 3D hydrogel scaffold modulus on osteoblast differentiation and mineralization revealed by combinatorial screening. *Biomaterials* **2010**, *31*, 5051−5062.
(54) Hassanajili, S.; Karami-Pour, A.; Oryan, A.; Talaei-Khozani, T. Preparation and characterization of PLA/PCL/HA composite scaffolds using indirect 3D printing for bone tissue engineering. *Mater. Sci. Eng.* **2019**, *104*, 109960.
(55) Dessì, M.; Borzacchiello, A.; Mohamed, T. H. A.; Abdel-Fattah, W. I.; Ambrosio, L. Novel biomimetic thermosensitive β-tricalcium phosphate/chitosan-based hydrogels for bone tissue engineering. *J. Biomed Mater. Res. A* **2013**, *101*, 2984−2993.

https://doi.org/10.1021/acs.chemmater.5c01899
Chem. Mater. 2025, 37, 9440−9450